Supporting Information for

Symmetry-Breaking Intramolecular Charge Transfer in the Excited State of *meso*-Linked BODIPY Dyads

Matthew T. Whited, Niral M. Patel, Sean T. Roberts, Kathryn Allen, Peter I. Djurovich, Stephen E. Bradforth, and Mark E. Thompson*

Department of Chemistry, University of Southern California, Los Angeles, California 90089

Experimental Section

General Considerations. 2-Methylpyrrole was obtained by a Wolff-Kishner reduction of pyrrole-2-carboxaldehyde,[1] as previously described by Lo and Fu.[2] Bis(5-methyl-1*H*-pyrrol-2-yl)methanone was prepared according to a literature procedure.[3] 8-Acetoxymethyl-4,4-difluoro-3,5-dimethyl-4-boro-3a,4a-diaza-s-indacene, 8-hydroxymethyl-4,4-difluoro-3,5-dimethyl-4-boro-3a,4a-diaza-s-indacene and 8-formyl-4,4-difluoro-3,5-dimethyl-4-boro-3a,4a-diaza-s-indacene were prepared according to a modified literature procedure.[4] All other reagents were purchased from commercial vendors and used without further purification. All air-sensitive manipulations were performed using standard Schlenk techniques as needed, following the procedures indicated below for each preparation. NMR spectra were recorded at ambient temperature on Varian Mercury 500 MHz and 600 MHz spectrometers. ^{1}H chemical shifts were referenced to residual solvent. UV–vis spectra were recorded on a Hewlett-Packard 4853 diode array spectrophotometer. Steady-state emission experiments were performed using a Photon Technology International QuantaMaster Model C-60SE spectrofluorimeter. Fluorescence lifetimes were determined through time-correlated single-photon counting measurements. Data that appear in Fig. S8 & S9 were recorded using an IBH Fluorocube lifetime instrument equipped with 405 nm (for dyad **2**) or 435 nm (for dyad **1**) LED excitation sources. The data in Fig. S10 was obtained using the frequency doubled output of a 250 kHz Ti:sapphire amplifier (Coherent RegA 9000) and a Becker and Hickl SPC 630 detection module. Quantum efficiency measurements were carried out using a Hamamatsu C9920 system equipped with a xenon lamp, calibrated integrating sphere and model C10027 photonic multichannel analyzer.

1,4-Bis(4,4-difluoro-3,5-dimethyl-4-bora-3a,4a-diaza-s-indacene-8-yl)benzene (1).

Terephthalaldehyde (762 mg, 5.68 mmol) and 2-methylpyrrole (2.03 g, 23.3 mmol) were dissolved in dry, degassed CH_2Cl_2 (40 mL) under N_2. The resulting solution was further degassed for 10 min, and trifluoroacetic acid (64 μL, 0.84 mmol) was added in two portions, causing the solution to darken immediately, and the reaction was allowed to proceed with stirring for 2 h. DDQ (2.58 g, 11.4 mmol) was added in one portion, causing an immediate color change to dark red-orange, and the resulting mixture was stirred for 13 h. *N*,*N*-Diisopropylethylamine (8.0 mL, 46 mmol) was added at once, causing a color change to dark brown, and stirring was continued for 15 min. Boron trifluoride diethyl etherate (8.0 mL, 64 mmol) was added slowly over the course of 1 min, causing the mixture to warm slightly. After 45 min, the mixture was quenched with $NaHCO_3$ (5% aq, 200 mL) and stirred vigorously for 2 h. Organics were removed and washed with Na_2SO_3 (10% aq, 2 × 100 mL), HCl (5% aq, 1 × 100 mL), and brine (2 × 100 mL). The organics were removed and dried with $MgSO_4$, filtered, and concentrated to a dark solid, which was purified by column chromatography (SiO_2 gel, $CHCl_3$ eluent, $R_f = 0.5$) to afford dyad **1** as a pure red-orange solid (200 mg, 7%). Crystals suitable for X-ray diffraction were obtained by chilling a concentrated solution of **1** in $CHCl_3$/hexane (1:1) overnight, and these were utilized for spectroscopic studies. UV-vis (CH_2Cl_2) λ_{max}: 350, 513. ^{1}H NMR ($CDCl_3$): δ 7.62 (s, 4H, phenylene Ar–*H*), 6.76 (d, $^3J_{HH}$ = 4.4 Hz, 4H, BODIPY Ar–*H*), 6.31 (d, $^3J_{HH}$ = 4.4 Hz, 4H, BODIPY Ar–*H*), 2.68 (s, 12H, –C*H*$_3$). ^{13}C NMR ($CDCl_3$): δ 158.38, 141.14, 135.94, 134.47, 130.41, 130.32, 119.91, 15.13. MALDI, *m*/*z* for $C_{28}H_{24}B_2F_4N_4$ calcd 514.21 (100%), 513.22 (51%), 515.22 (33%); found 512.83 (100%), 511.83 (51%), 513.82 (45%). HRMS for $C_{28}H_{25}B_2N_4F_4$ (MH+) calcd 515.2196, found 515.2197.

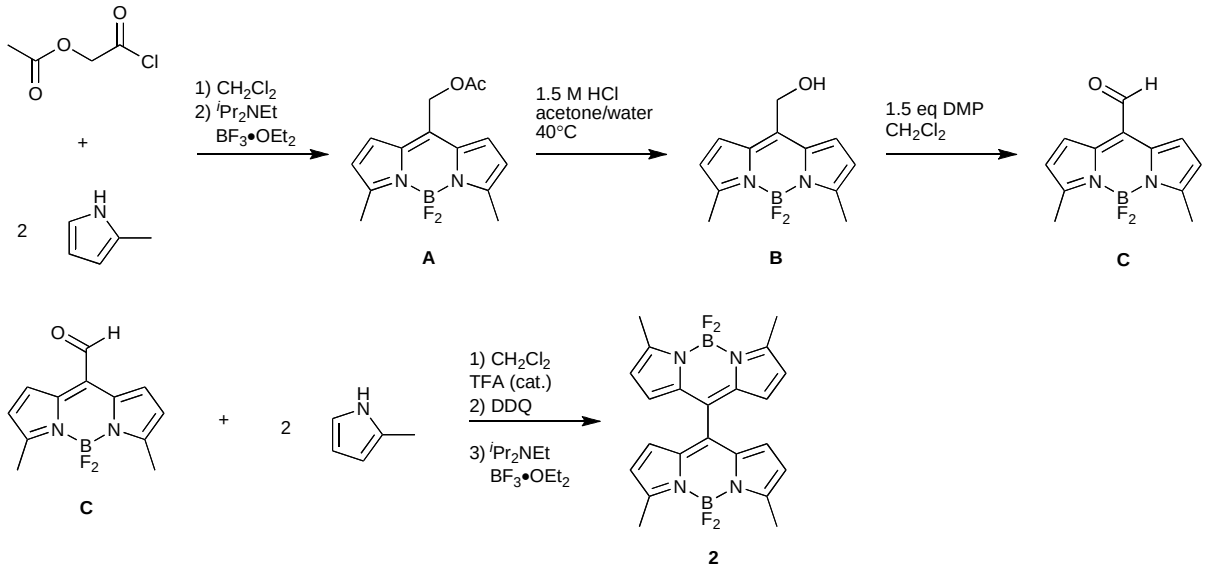

8-Acetoxymethyl-4,4-difluoro-3,5-dimethyl-4-boro-3a,4a-diaza-s-indacene (A). 2-Methylpyrrole (2.01 g, 24.8 mmol) was dissolved in dry, degassed CH_2Cl_2 (20 mL) in an oven-dried three-necked flask that had been purged with N_2. The solution was cooled to 0 °C and acetoxyacetyl chloride (2.02 g, 14.8 mmol) was added in one portion in the dark and the reaction was allowed to proceed with stirring for 1 h, during which time the color turned dark red. *N*,*N*-Diisopropylethylamine (8.58 mL, 49.3 mmol) was added at room temperature, causing a color change to clear orange, and stirring was continued for 30 min followed by dropwise addition of BF_3•OEt_2 (6.18 mL, 49.3 mmol). During addition of BF_3•OEt_2 the color changed to dark red. The reaction was left stirring for 30 min and then was concentrated and purified by flash chromatography (SiO_2 gel, 25 % CH_2Cl_2/hexanes, $R_f = 0.14$) to yield the product as a gold-pink solid (235 mg, 11 %). ^{1}H NMR ($CDCl_3$, 600 MHz): δ 7.18 (d, $^3J_{HH} = 4.2$ Hz, 2H, BODIPY Ar–*H*), 6.30 (d, $^3J_{HH} = 4.2$ Hz, 2H, BODIPY Ar–*H*), 5.22 (s, 2H, –C*H*$_2$), 2.62 (s, 6H, –C*H*$_3$), 2.09 (s, 3H, –COC*H*$_3$). ^{13}C NMR ($CDCl_3$, 600 MHz): δ 170.20, 158.96, 134.60, 133.97, 127.98, 119.84, 59.11, 20.85, 14.98. HRMS for $C_{14}H_{16}BN_2O_2F_2$ (MH+) calcd 293.1267, found 293.1261.

8-Hydroxymethyl-4,4-difluoro-3,5-dimethyl-4-boro-3a,4a-diaza-s-indacene (B). **A** (350 mg, 1.20 mmol) was dissolved in acetone (60 mL) and a solution of 4 M HCl (36 mL) was added. A condenser was fitted to the flask and the reaction was heated to 40 °C until the solution turned green and the TLC showed no starting material. The crude mixture was diluted with CH_2Cl_2, washed with water (2 × 75 mL), saturated $NaHCO_3$ (2 × 75 mL) and the organic layer was removed, dried over $MgSO_4$, filtered, concentrated and purified by flash chromatography (SiO_2 gel, CH_2Cl_2, $R_f = 0.16$) to afford the product as a red-gold solid (210 mg, 71 %). ^{1}H NMR ($CDCl_3$, 600 MHz): δ 7.23 (d, $^3J_{HH} = 4.2$ Hz, 2H, BODIPY Ar–*H*), 6.97 (s, 1H, –O*H*), 6.27 (d, $^3J_{HH} = 4.2$ Hz, 2H, BODIPY Ar–*H*), 4.79 (s, 2H, –CH_2), 2.60 (s, 6H, –CH_3). ^{13}C NMR ($CDCl_3$, 600 MHz) δ 158.41, 139.17, 133.97, 127.59, 119.53, 59.45, 14.93. HRMS for $C_{12}H_{14}BN_2OF_2$ (MH+) calcd 251.1162, found 251.1167.

8-Formyl-4,4-difluoro-3,5-dimethyl-4-boro-3a,4a-diaza-s-indacene (C). **B** (200 mg, 0.8 mmol) was dissolved in dry, degassed CH_2Cl_2 (15 mL) and was cannulated into a solution of Dess-Martin periodinane (509 mg, 1.20 mmol) in dry, degassed CH_2Cl_2 (15 mL) at 0 °C. The solution was allowed to warm to room temperature and left stirring for 1 h. When the TLC showed no starting material the reaction was quenched with saturated $Na_2S_2O_3$ (50 mL), washed with saturated $NaHCO_3$ (2 × 50 mL) and water (2 × 50 mL). The organic layer was removed, dried over $MgSO_4$, filtered and concentrated, then purified by passing through a plug of SiO_2 gel with CH_2Cl_2 ($R_f = 0.38$). The product collected was a dark purple solid (164 mg, 83%). ^{1}H NMR ($CDCl_3$, 600 MHz): δ 10.33 (s, 1H, –C*H*O), 7.51 (d, $^3J_{HH} = 4.2$ Hz, 2H, BODIPY Ar–*H*), 6.40 (d, $^3J_{HH} = 4.2$ Hz, 2H, BODIPY Ar–*H*), 2.65 (s, 6H, –CH_3). ^{13}C NMR ($CDCl_3$, 600 MHz) δ

188.75, 161.39, 134.87, 129.74, 125.87, 121.86, 15.33. HRMS for $C_{12}H_{12}BN_2OF_2$ (MH+) calcd 249.1005, found 249.1008.

Bis(4,4-difluoro-3,5-dimethyl-4-bora-3a,4a-diaza-s-indacene-8-yl) (2). **C** (36 mg, 0.15 mmol) was dissolved in dry, degassed CH_2Cl_2 (10 mL) and 2-methylpyrrole (24 mg, 0.29 mmol) was added. The reaction was monitored by TLC until no starting material remained. DDQ (33 mg, 0.15 mmol) was added in one portion and the reaction was monitored by TLC until the condensation product was consumed. *N*,*N*-Diisopropylethylamine (0.10 mL, 0.58 mmol) was added in one portion, followed after 15 min by dropwise addition of $BF_3{\bullet}OEt_2$ (0.07 mL, 0.6 mmol). The reaction was left stirring for 15 min and then was quenched with saturated $Na_2S_2O_3$ (25 mL), washed with saturated $NaHCO_3$ (2 × 50 mL) and the organic layer was removed. The crude mixture was dried over $MgSO_4$, filtered and passed through a plug of SiO_2 gel using CH_2Cl_2 ($R_f = 0.33$) to recover a dark pink-green solid (25 mg, 38 %). UV-vis (CH_2Cl_2) λ_{max}: 334, 530. ^{1}H NMR ($CDCl_3$, 400 MHz): δ 6.84 (d, $^3J_{HH} = 4.4$ Hz, 4H, BODIPY Ar–*H*), 6.23 (d, $^3J_{HH} = 4.4$ Hz, 4H, BODIPY Ar–*H*), 2.65 (s, 12H, –C*H*$_3$). ^{13}C NMR ($CDCl_3$, 600 MHz) δ 159.55, 135.04, 131.87, 130.06, 120.13, 15.06. HRMS for $C_{22}H_{21}B_2N_4F_4$ (MH+) calcd 439.1883, found 439.1893.

Computational Methods. All of the molecular calculations were performed with the Titan (version 1.0.7) software package at the B3LYP level using a 6-31g* basis set.

Femtosecond Transient Absorption Spectroscopy. Femtosecond transient absorption measurements were performed using a Ti:sapphire regenerative amplifier (Coherent Legend, 3.5 mJ, 35 fs, 1kHz repetition rate). Approximately 10% of the amplifier output was used to pump a type II OPA (Spectra Physics OPA-800C) resulting in the generation of excitation pulses

centered on average at 509 nm with 13.2 nm of bandwidth. At the sample position, the pump was lightly focused to a spot size of 0.3 mm (FWHM) using a CaF_2 lens. Probe pulses were generated by focusing a small amount of the amplifier output into a rotating CaF_2 plate, yielding a supercontinuum spanning the range of 320–950 nm. A pair of off-axis aluminum parabolic mirrors collimated the supercontinuum probe and focused it into the sample.

Data were collected for perpendicularly oriented pump and probe to allow for the suppression of scattered excitation light by passing the probe through an analyzing polarizer after the sample. A spectrograph (Oriel MS127I) dispersed the supercontinuum probe onto a 256 pixel silicon diode array (Hamamatsu), enabling multiplex detection of the transmitted probe as a function of wavelength. Differential detection of pump-induced changes in the probe was achieved with an optical chopper that blocked every other pump pulse. The transient spectra reported in both the main text and supporting information represent the average probe transmission change measured for 1500 on/off pump pulse pairs.

Samples containing **2** dissolved in either toluene, dichloromethane, or acetonitrile were held in a 1 mm pathlength cuvette. Due to a tendency of **1** to photodegrade in air, samples of this compound were contained in a custom 1 cm pathlength quartz cuvette kept under nitrogen atmosphere. The concentration of each sample was adjusted to give a peak optical density between 0.10 and 0.18. During data collection, the samples were slowly oscillated perpendicular to the pump and probe to aid in the dispersal of heat deposited in the sample by the pump. At early time delays, a strong nonresonant signal from the sample cell and solvent is observed. For spectra measured in the thinner 1 mm cell, the solvent response is found to relax within 170 fs, but persists for ~300 fs for data measured in the thicker 1 cm cuvette. To suppress this nonresonant signal, a second measurement of an identical cuvette containing just neat solvent

was performed after measuring spectra for either dyad. The transient signal resulting from this reference sample was then subtracted from the dyad signal. The nonresonant solvent response also provided a measure of the temporal dispersion of the supercontinuum probe resulting from propagation through the CaF_2 plate and sample. The presented data have been corrected to account for this dispersion.

The transient data presented in the main text of **1** and **2** in acetonitrile were carried out using pump fluences of 230 and 470 $\mu J/cm^2$, respectively. Measurements made using fluences of 10%, 30%, and 50% of these values scaled linearly with the higher fluence data and yielded similar fit time constants, suggesting that two photon absorption and sample degradation do not contribute to the signal. The transient spectra that appear below for **1** in toluene were measured using a pump fluence of 95 $\mu J/cm^2$. This value was increased for experiments in dichloromethane, which used a fluence of 230 $\mu J/cm^2$. Spectra of **2** were recorded using similar fluences, 150 and 190 $\mu J/cm^2$ for toluene and dichloromethane, respectively.

Global Analysis of Transient Absorption Spectra. Our transient spectra indicate that the initially excited S_1 population of **1** evolves over time to form an ICT state that nonradiatively returns to the ground state while for **2** the ICT state persists long enough to allow some molecules to relax radiatively. Moreover, the rate of formation of the ICT state and its subsequent relaxation to the ground state are found to depend strongly on the polarity of the surrounding medium. To quantify how these rates change as a function of solvent polarity, we have fit the transient spectra obtained for **1** and **2** in acetonitrile, dichloromethane, and toluene to a linear decomposition model that has been described in detail elsewhere.[5-7] Briefly, this model

assumes that the data can be decomposed linearly as a set of time independent decay associated difference spectra (DADS),[8-9] $\{\sigma_n(\lambda)\}$, with time varying amplitudes, $\{c_n(t)\}$:

$$S(\lambda,t) = \sum_n c_n(t)\sigma_n(\lambda). \quad \text{(S1)}$$

Each DADS represents the characteristic transient absorption spectrum measured for a given excited configuration of the system. These basis spectra contain positive features due to excited state absorption and negative peaks due to a combination of stimulated emission and ground state depopulation (bleaching).

To calculate $\{c_n(t)\}$, we assume that the evolution of the initially excited population is governed by a series of sequential first order rate processes:

$$c_1(t) \xrightarrow{k_1} c_2(t) \xrightarrow{k_2} c_3(t) \xrightarrow{k_3} \ldots . \quad \text{(S2)}$$

The time dependent behavior of $\{c_n(t)\}$ is given from the solution to the set of coupled differential equations implied by Eq. S2:

$$\begin{aligned} \frac{dc_1(t)}{dt} &= I_0 - k_1 c_1(t) \\ \frac{dc_n(t)}{dt} &= k_{n-1}c_{n-1}(t) - k_n c_n(t), \; n \neq 1, \end{aligned} \quad \text{(S3)}$$

where I_0 is the initial population placed in the excited state by the excitation pulse. In general, any first order process that modifies the transient spectrum can be accounted for through the inclusion of an additional DADS. For each measured transient spectrum, a least squares minimization routine was used to find the minimal number of DADS required to reproduce the data set. The resulting DADS and fits to the transient spectra are plotted in Fig. S4 and S6.

Since the transient spectra presented below were collected for perpendicularly oriented pump and probe, changes in the spectra with time can result from diffusive reorientation of the excited

dyad in addition to transitions between electronic states. In the analysis scheme described above, spectral changes arising from reorientation produce an additional DADS that only modifies the amplitudes of spectral features that appear in the preceding DADS.

Excited State Dynamics of Dyads 1 and 2. Fig. S3 plots a summary of the transient spectra recorded for **1** in acetonitrile, dichloromethane, and toluene. As noted in the main text, in acetonitrile we observe two kinetic processes. An induced absorption band peaked at 545 nm assigned to BODIPY radicals appears with a time constant of 4.8 ps, signaling formation of an ICT state. Following the growth of this band, all spectral features decay with a time constant of 34 ps due to nonradiative relaxation to the ground state. Only two DADS are required to model these processes (Fig. S4a). We interpret these DADS as the characteristic transient spectral signatures of the initially populated S_1 excited state (σ_1) and subsequently formed ICT state (σ_2).

Transient spectra of **1** measured in the less polar solvent dichloromethane show qualitatively similar behavior to data recorded in acetonitrile, but formation of the ICT state and relaxation to the ground state occur over much longer time scales, 18 ps and 1.6 ns respectively. In toluene, a narrowing of the photobleach/stimulated emission lineshape is seen at early delays. We tentatively assign this feature to a dynamic Stokes shift of the S_1 emission lineshape resulting from nonpolar solvation and model it with a 1.0 ps time constant. Following this process, all features in the transient spectrum relax with the same rate, implying that the ICT state is not populated in toluene. The DADS analysis yields a relaxation time scale of 860 ps that closely matches the S_1 life time determined from TCSPC measurements (Fig S7). The DADS fit also accounts for the diffusive reorientation of the dyad, which is found to occur with a time constant of 75 ps.

A summary of the transient spectra measured for **2** is plotted Fig. S5, while the DADS used to fit these spectra appear in Fig. S6. In acetonitrile, growth of the ICT state of **2** occurs much faster than that of **1**, taking place within the time resolution of our experiment ($1/k_{ICT} \leq 175$ fs). Once formed, the ICT state of 2 persists for an order of magnitude longer than that of **1**, relaxing with a time constant of 650 ps. To model this process, we utilize three DADS, two to account for the transient absorption lineshapes indicative of the S_1 and ICT states, and an additional DADS to account for the diffusive reorientation of dyad **2** (37 ps). Note, the diffusive reorientation of **1** in acetonitrile did not enter into our analysis since the nonradiative relaxation **1** occurs on a time scale faster than that expected for diffusive reorientation.

Similar to **1**, in dichloromethane **2** shows time scales slower than those obtained in acetonitrile for formation of the ICT state and relaxation to the ground state (490 fs and 6.7 ns, respectively). Diffusive reorientation is found to occur with 52 ps time constant. Since the ICT state of **2** is emissive, time resolved fluorescence experiments (Fig. S8) were used to constrain the life time of the ICT state for the purposes of fitting.

In contrast to the behavior seen for **1**, transient spectra of **2** in toluene show a loss of stimulated emission from the S_1 state at 590 nm over the course of a few picoseconds. Given the larger driving force for ICT formation for **2** with respect to **1** as revealed by our cyclic voltammetry measurements, we interpret this stimulated emission loss as an indication that 2 forms an ICT state in toluene despite the nonpolar nature of this solvent. The time scale for formation of the ICT state extracted from the DADS analysis is 4.5 ps but its lifetime could not be determined since the transient spectra show no evolution following the formation of this state. As with **1** in toluene, to fully reproduce the spectra, a narrowing of the photobleach at short

delays needed to be included in the DADS analysis (800 fs) as well as diffusive reorientation by **2** (62 ps).

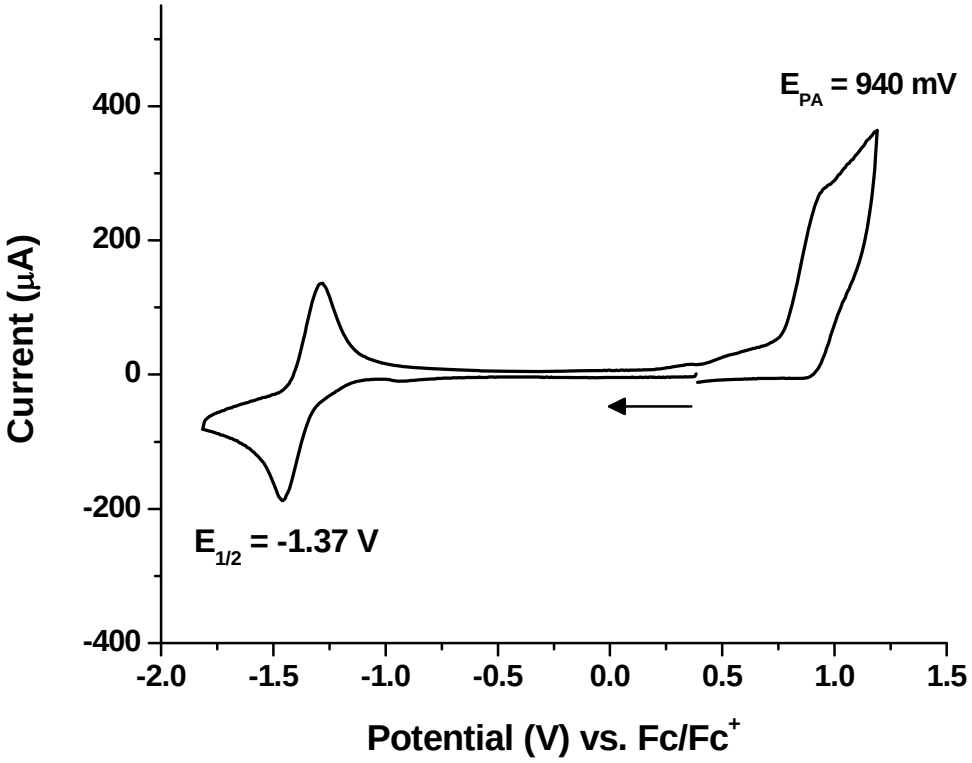

Figure S1. Cyclic voltammogram of dyad **1** in CH_2Cl_2 ($^nBu_4NPF_6$ electrolyte; 50 mV/s scan rate).

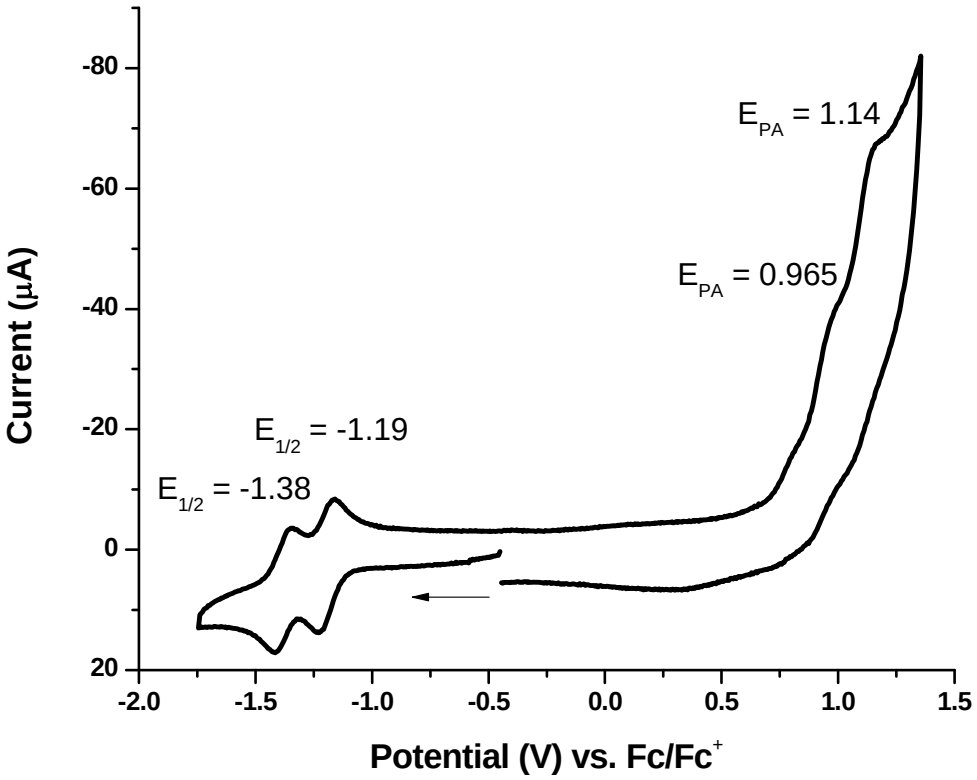

Figure S2. Cyclic voltammogram of dyad **2** in CH_2Cl_2 ($^nBu_4NPF_6$ electrolyte; 50 mV/s scan rate).

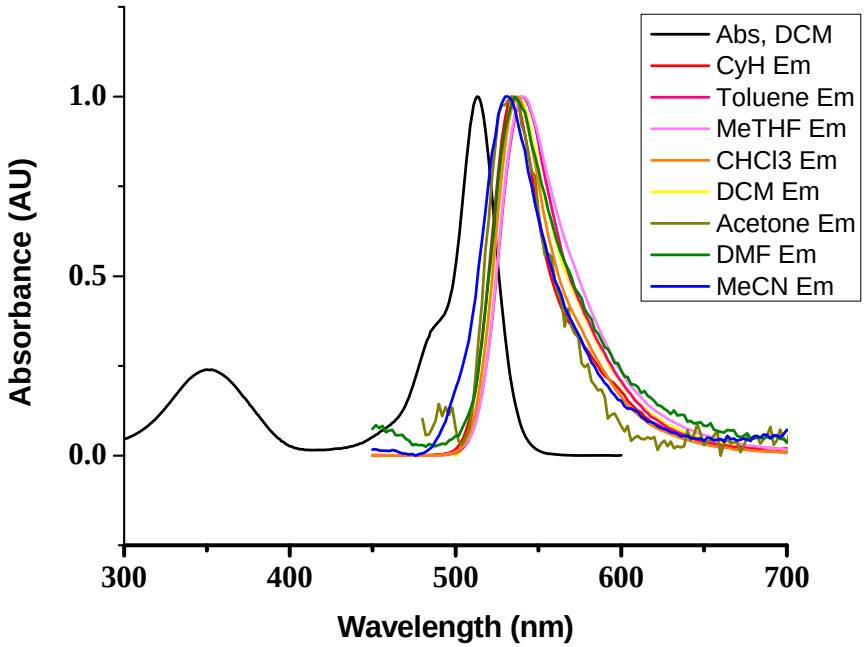

Figure S3. Absorbance and emission spectra of dyad **1** in various solvents.

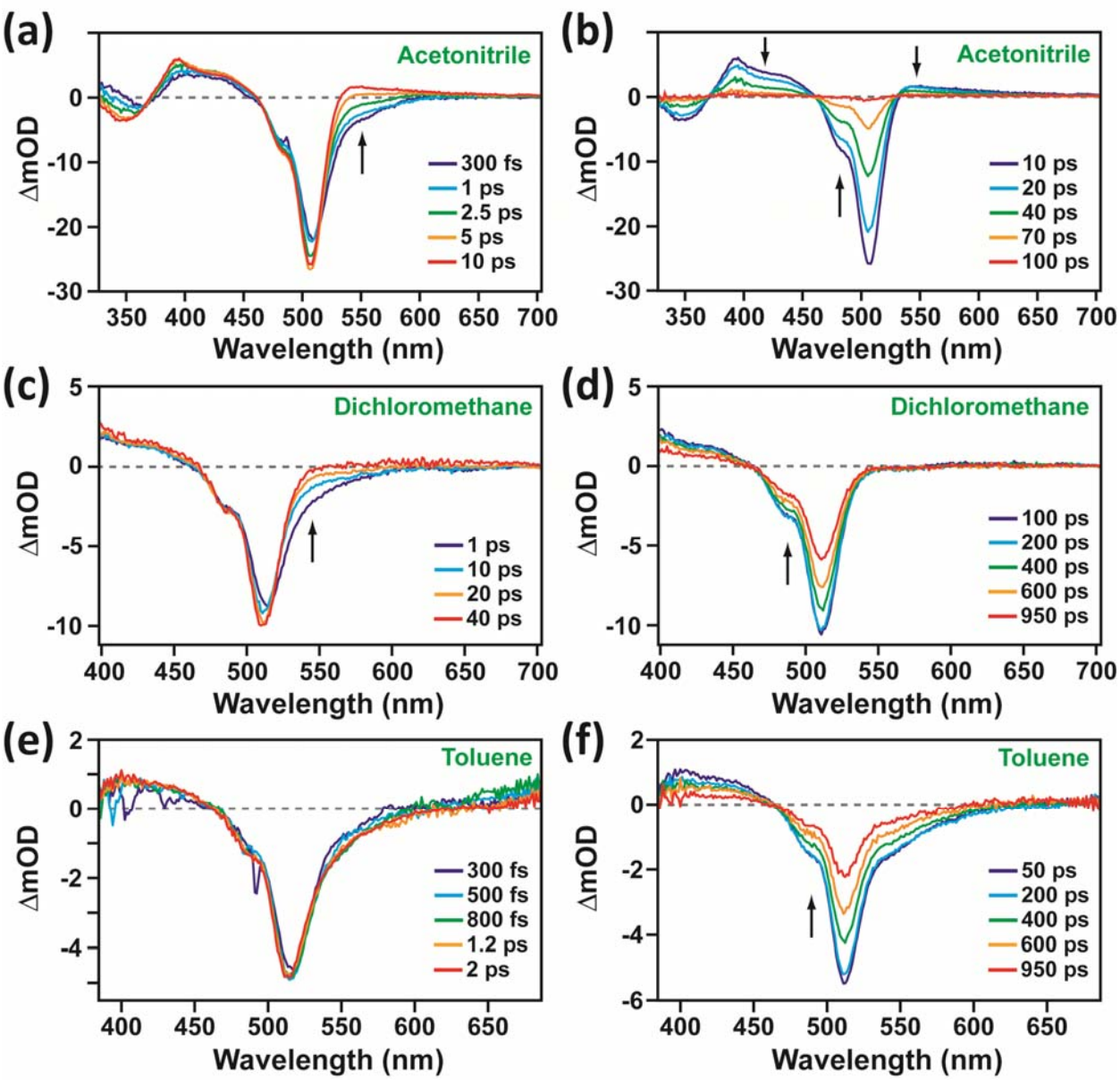

Figure S4. Transient absorption of dyad **1** in acetonitrile (a & b), dichloromethane (c & d), and toluene (e & f). Formation of an ICT state is observed in both acetonitrile and dichloromethane, but is not seen in toluene. The sharp features that occur in the toluene data set below 500 nm at Δt = 300 fs result from an imperfect subtraction of the background solvent response.

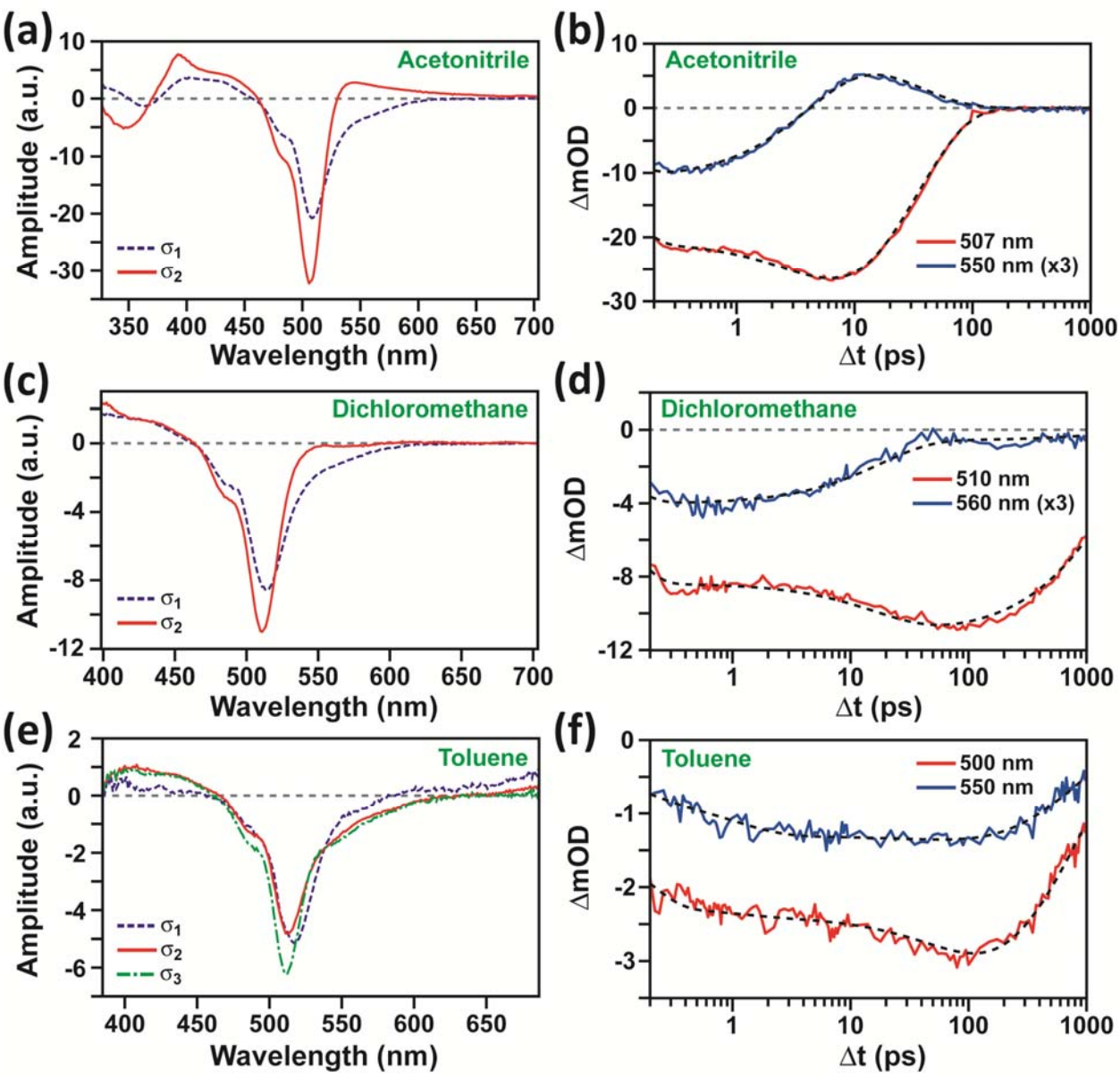

Figure S5. (a, c, e) DADS used to reproduce the transient spectra of dyad **1** plotted in Fig. S3. (b, d, f) Slices taken through the ground state bleach of each dyad (red) and spectral range indicative of BODIPY radical absorption (blue) alongside fits based on DADS analysis (black dashed).

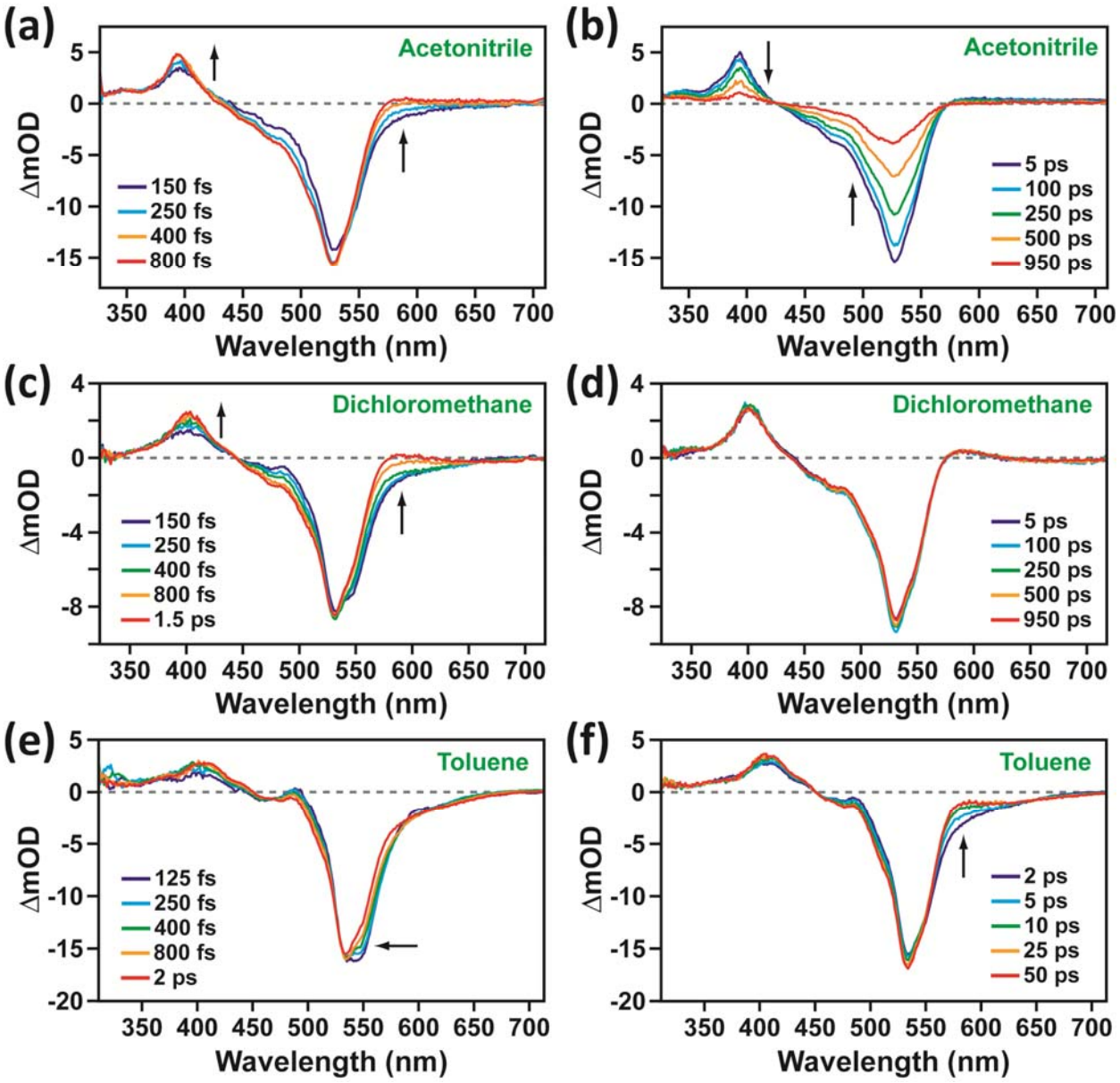

Figure S6. Transient absorption of dyad **2** in acetonitrile (a & b), dichloromethane (c & d), and toluene (e & f). Formation of an ICT state is observed in each solvent and occurs more rapidly than for dyad **1**.

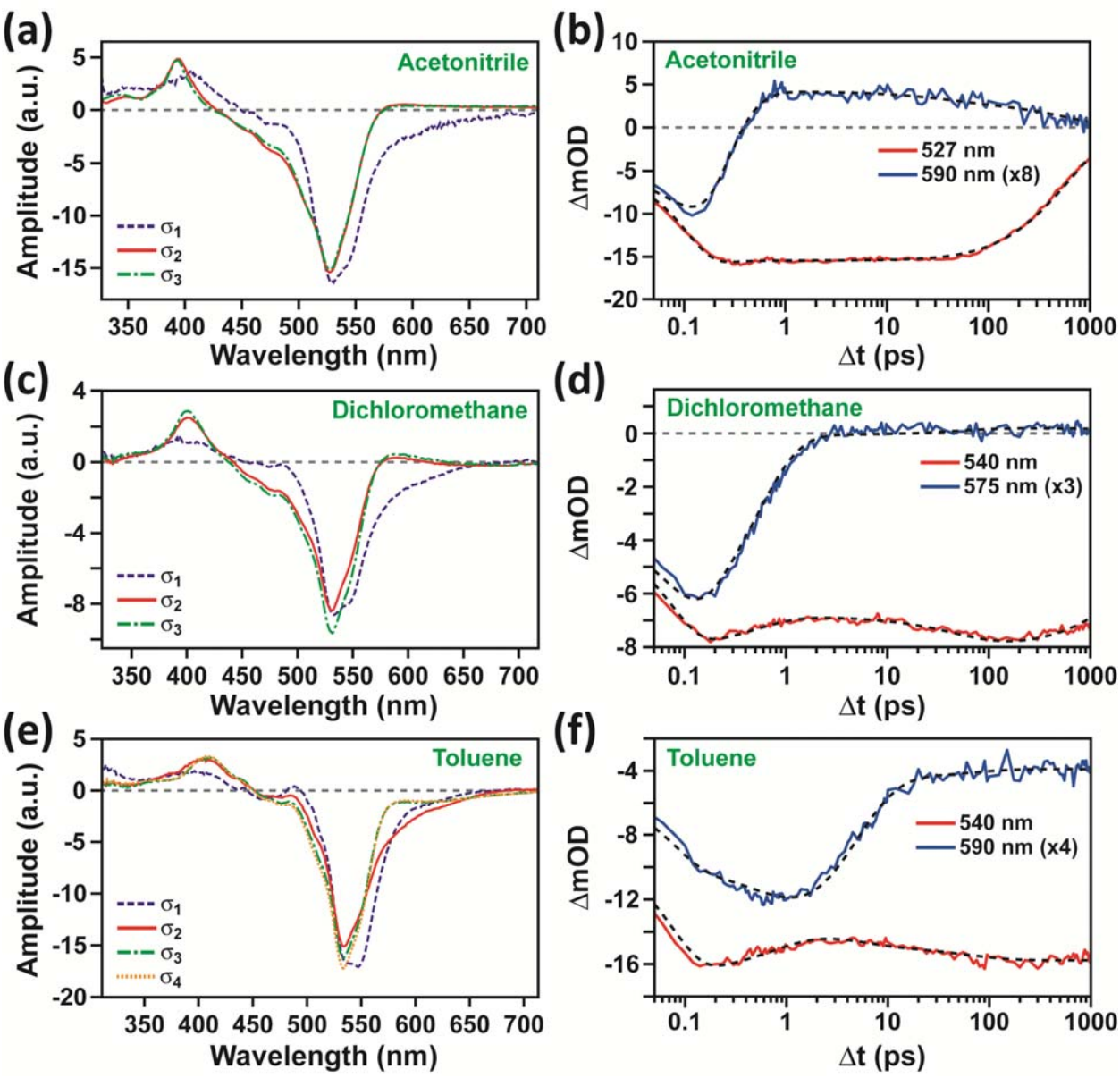

Figure S7. (a, c, e) DADS used to reproduce the transient spectra of dyad **2** plotted in Fig. S5. (b, d, f) Slices taken through the ground state bleach of each dyad (red) and spectral range indicative of BODIPY radical absorption (blue) along with fits based on DADS analysis (black dashed).

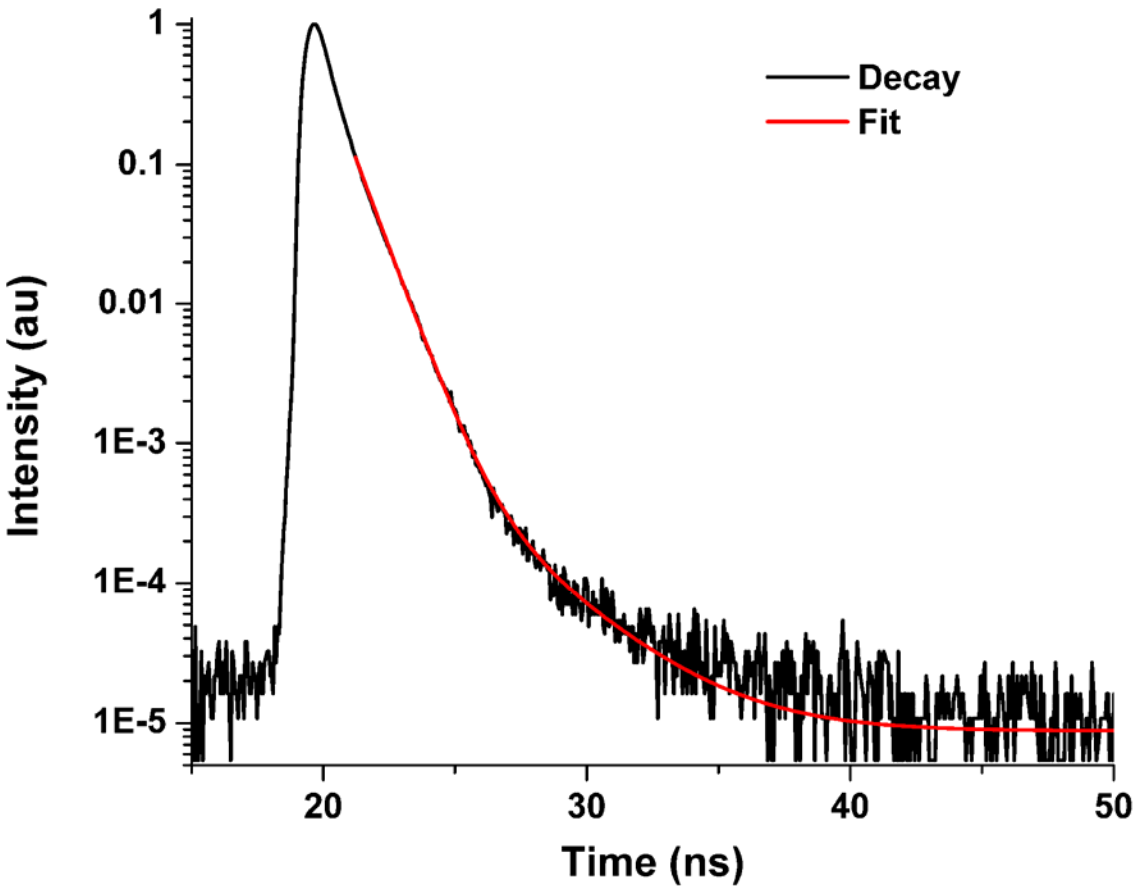

Figure S8. Normalized emission decay of dyad **1** in toluene (535 nm) with biexponential fit including a major short (845 ps, 96%) and minor long (2.76 ns, 4%) component following excitation at 435 nm.

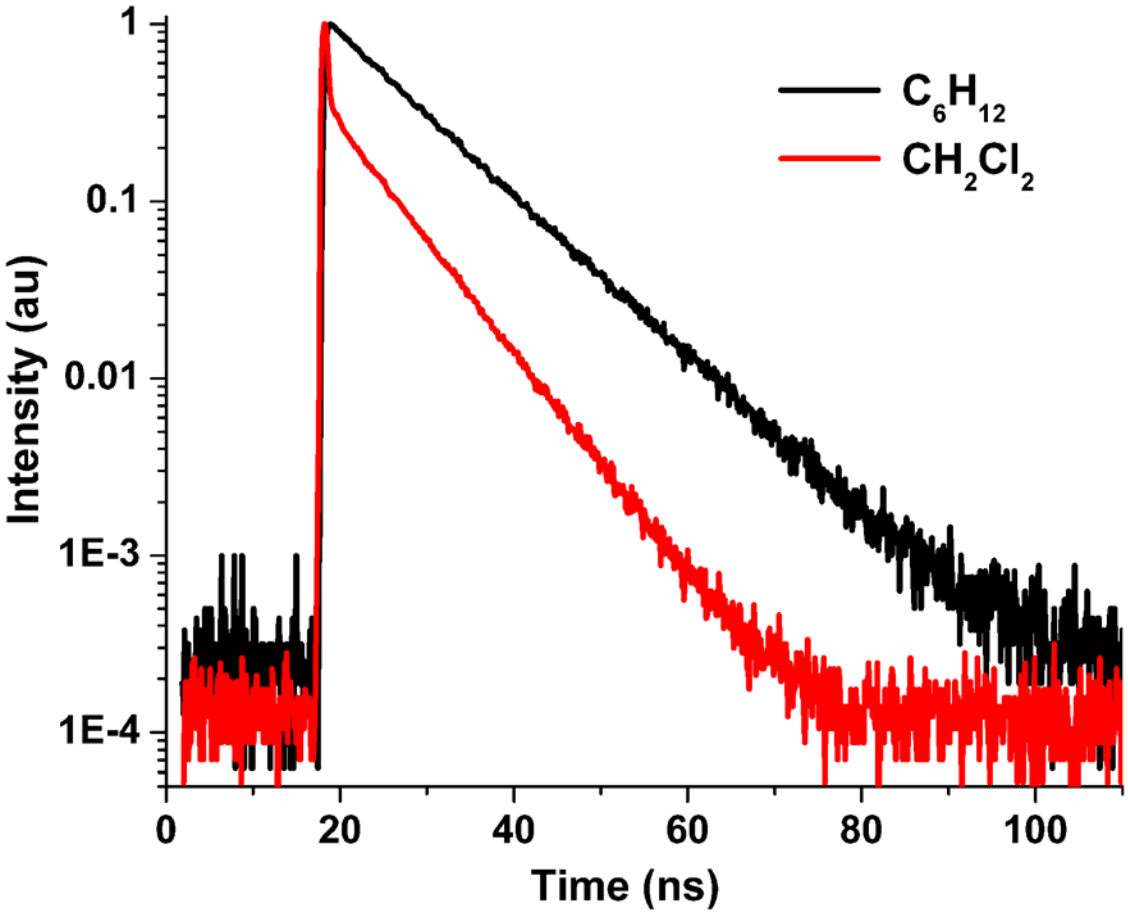

Figure S9. Normalized emission decays of dyad **2** in cyclohexane (563 nm) and dichloromethane (563 nm) following excitation at 405 nm.

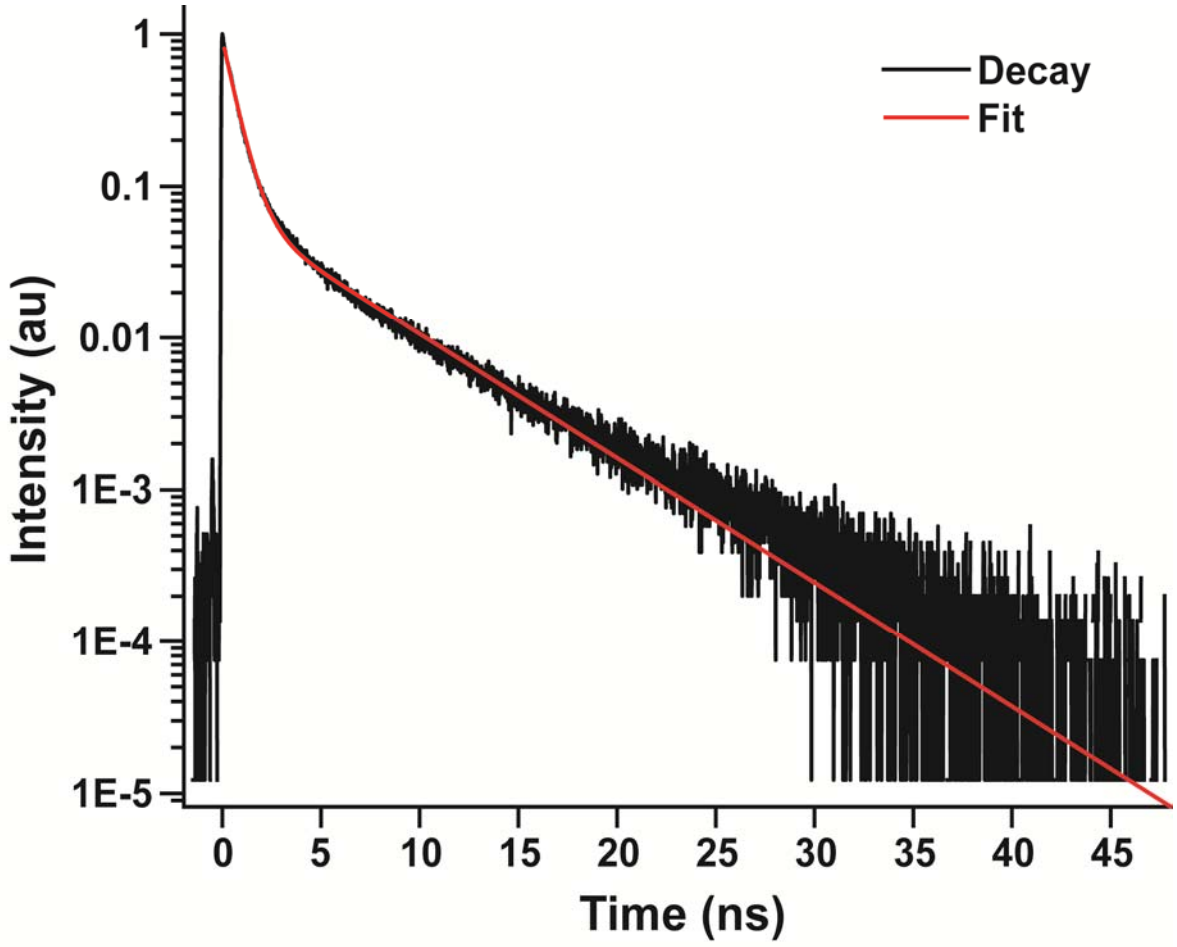

Figure S10. Normalized emission decay of dyad **2** in acetonitrile (750 nm) following excitation at 400 nm. The data fits well to a biexponential decay with a major component (680 ps, 92.5%) due to ICT emission and a minor component (5.3 ns, 7.5%) that results from BODIPY monomer impurities.

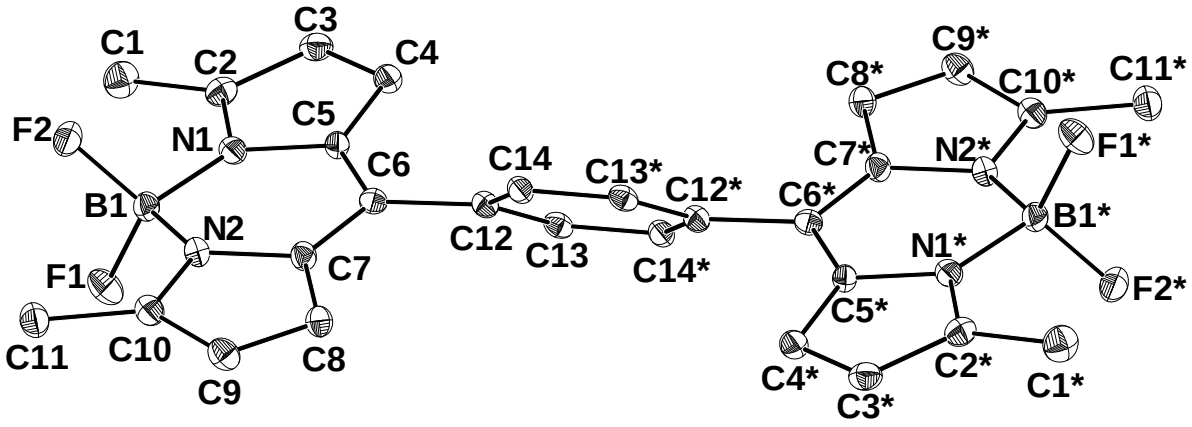

Figure S11. Fully labeled X-ray structure of dyad **1**.

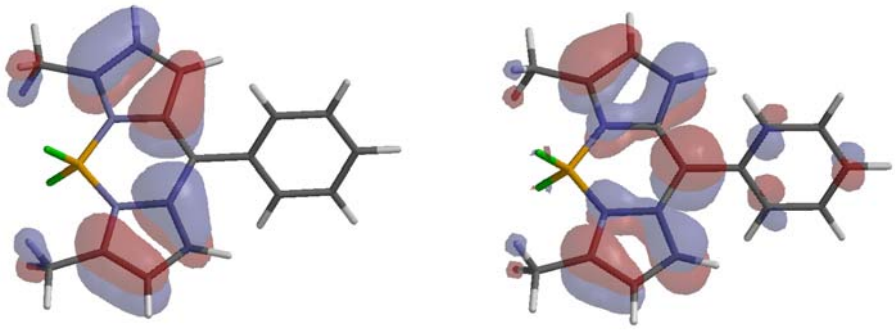

Figure S12. Surface contours for the HOMO (left) and LUMO (right) of 3,5-Me_2BOPDIPY-Ph.

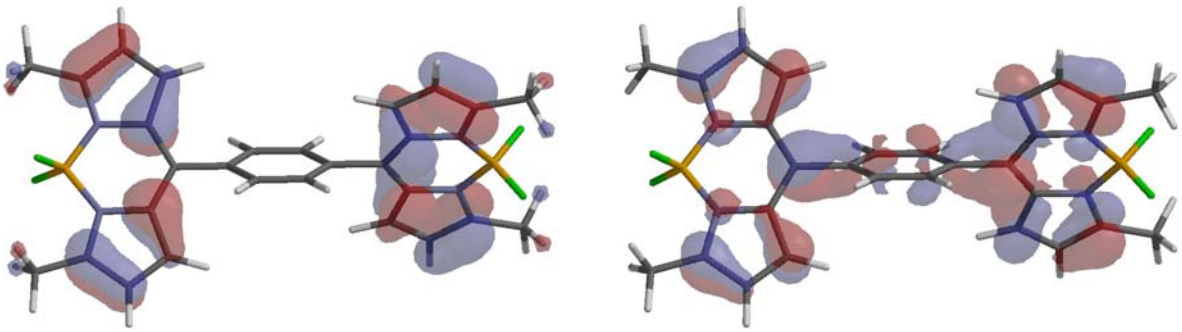

Figure S13. Surface contours for the HOMO (left) and LUMO (right) of dyad **1**.

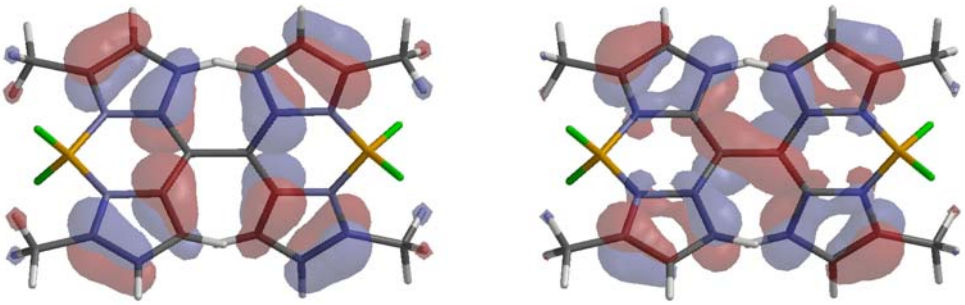

Figure S14. Surface contours for the HOMO (left) and LUMO (right) of dyad **2**.

Table S1. Crystal data and structure refinement for dyad **1**

Identification code	mtw04
Empirical formula	C28 H24 B2 F4 N4
Formula weight	514.13
Temperature	123(2) K
Wavelength	0.71073 Å
Crystal system	Orthorhombic
Space group	Pbca
Unit cell dimensions	a = 12.808(3) Å α= 90°.
	b = 12.205(2) Å β= 90°.
	c = 15.019(3) Å γ = 90°.
Volume	2347.8(8) Å^3
Z	4
Density (calculated)	1.455 Mg/m^3
Absorption coefficient	0.108 mm^{-1}
F(000)	1064
Crystal size	0.10 x 0.09 x 0.07 mm^3
Theta range for data collection	2.67 to 27.55°.
Index ranges	-16<=h<=16, -10<=k<=15, -19<=l<=18
Reflections collected	13598
Independent reflections	2688 [R(int) = 0.1065]
Completeness to theta = 25.00°	100.0 %
Absorption correction	Semi-empirical from equivalents
Max. and min. transmission	0.7456 and 0.5788
Refinement method	Full-matrix least-squares on F^2
Data / restraints / parameters	2688 / 0 / 174
Goodness-of-fit on F^2	1.119
Final R indices [I>2sigma(I)]	R1 = 0.0571, wR2 = 0.0838
R indices (all data)	R1 = 0.1215, wR2 = 0.0926
Largest diff. peak and hole	0.285 and -0.209 e.Å^{-3}

References

1. R. M. Silverstein, E. E. Ryskiewicz and C. Willard, *Org. Synth.*, 1956, **36**, 74-77.
2. M. M. C. Lo and G. C. Fu, *J. Am. Chem. Soc.*, 2002, **124**, 4572-4573.
3. P. S. Clezy and G. A. Smythe, *Aust. J. Chem.*, 1969, **22**, 239-&.
4. K. Krumova and G. Cosa, *J. Am. Chem. Soc.*, 2010, **132**, 17560-17569.
5. M. Vengris, M. A. van der Horst, G. Zgrablic, I. H. M. van Stokkum, S. Haacke, M. Chergui, K. J. Hellingwerf, R. van Grondelle and D. S. Larsen, *Biophys. J.*, 2004, **87**, 1848-1857.
6. X. Chen, D. S. Larsen, S. E. Bradforth and I. H. M. v. Stokkum, *J. Phys. Chem. A*, 2011, **115**, 3807-3819.
7. S. T. Roberts, C. W. Schlenker, V. Barlier, R. E. McAnally, Y. Y. Zhang, J. N. Mastron, M. E. Thompson and S. E. Bradforth, *J. Phys. Chem. Lett.*, 2011, **2**, 48-54.
8. J.-E. Löfroth, *J. Phys. Chem.* 1986, **90**, 1160-1168.
9. I. H. M. van Stokkum, D. S. Larsen, R. van Grondelle, *Biochim. Biophys. Acta.*, 2004, **1657**, 82-104.